ChemComm

COMMUNICATION

View Article Online
View Journal | View Issue

Cite this: *Chem. Commun.*, 2023, 59, 4616

Received 12th January 2023,
Accepted 6th March 2023

DOI: 10.1039/d3cc00179b

rsc.li/chemcomm

Unprecedented highly efficient photoluminescence in a phosphorescent Ag(I) coordination polymer†

Haruka Yoshino, *[a] Masaki Saigo,[b] Kiyoshi Miyata, [b] Ken Onda, [b] Jenny Pirillo, [c] Yuh Hijikata, [c] Wataru Kosaka [a] and Hitoshi Miyasaka *[a]

A luminescent three-dimensional coordination polymer (CP) of $[Cd^{II}(pmd)\{Ag^{I}(CN)_2\}_2]$ (1; pmd = pyrimidine) comprising two different coordination modes of Ag^+ ions was synthesised herein. 1 exhibited thermochromic luminescence, accompanied by positive thermal elongation of the Ag···Ag distance. Moreover, 1 showed a bright phosphorescence with the highest photoluminescence quantum yield (Φ_{em}), approximately 60% at room temperature, among previously reported phosphorescent Ag-based CPs or metal–organic frameworks.

Emission-switchable luminescent materials are at the forefront of technological innovations owing to their potential applications in sensitive sensors, image displays, and fluorescent thermometers.[1–5] However, the practical application of emission materials requires the fulfilment of multiple criteria, including structural stability, facile and cost-effective fabrication, and high quantum efficiency. Notably, Ag-based luminescent materials have received considerable attention because of their attractive characteristics: (i) affordability, (ii) low toxicity and biocompatibility, (iii) outstanding luminescence properties, and (iv) sensing abilities.[6–10] For instance, an Ag cluster-assembled material (SCAM) of $[Ag_{12}(StBu)_6(CF_3COO)_6(CPPP)_2(dimethylacetamide)_{12}]_n$ (CPPP = 2,5-bis(4-cyanophenyl)-1,4-bis(4-(pyridine-4-yl)-phenyl)-1,4-dihydropyrrolo[3,2-*b*]pyrrole) exhibited an enhancement of luminescence efficiency compared with that of the CPPP ligand owing to rigidifying methodology through matrix coordination induced emission effects.[11] More recently, the development of highly emissive Ag-thermally activated delayed fluorescence (TADF) complexes was demonstrated, which was attributed to the narrow singlet (S_1)–triplet (T_1) energy gaps, hybrid local excitation and charge transfer (CT) characters facilitating inverse intersystem crossing, and molecular rigidity.[12] Hence, Ag-based compounds are promising candidates for fabricating sustainable and high-performance luminescent materials.

Luminescent coordination polymers (CPs) and metal–organic frameworks (MOFs), a new class of crystalline porous and functional materials, are being extensively developed in the field of materials science.[13–22] In particular, Ag-CPs/MOFs have great potential as platforms for novel photofunctional materials. For example, a study reported the advantages of MOFs in device applications such as light-emitting diodes, including the facile preparation and highly designability of the frameworks.[23] However, Ag-CPs/MOFs still have an unresolved challenge of low photoluminescence quantum yield (Φ_{em}) at RT, which hinders their wide applications at this stage. Therefore, development of high-performance Ag-based emission materials is required to improve luminescence efficiency.

Herein, we report a novel phosphorescent Ag-CP that exhibits an intense light-blue emission with the highest Φ_{em} value of 60% at RT. The luminescence features of the resultant CP were studied by variable-temperature (VT) X-ray diffraction, photoluminescence measurements, and density functional theory (DFT) calculations.

$[Cd^{II}(pmd)[Ag^{I}(CN)_2]_2$ (**1**; pmd = pyrimidine) was synthesised by a slow-diffusion method using an aqueous solution of $Cd(NO_3)_2{\cdot}4H_2O$, pmd, and $K[Ag(CN)_2]$, yielding colourless single crystals (Fig. S1(d)–(f), ESI†). A detailed synthesis of **1** is provided in the ESI.† Single-crystal X-ray diffraction (SCXRD) analysis revealed that compound **1** crystallised in the monoclinic space group *C*2/*c*, and the crystal parameters are listed in Table S1 (ESI†). The framework of **1** contains Cd–CN–Ag linkages, which are bridged by bidentate pmd ligands and Ag^+ ions, forming a highly dense 3D structure (Fig. 1, Table S1 and

[a] *Institute for Materials Research, Tohoku University, 2-1-1 Katahira, Aoba-ku, Sendai 980-8577, Japan. E-mail: haruka.yoshino.a2@tohoku.ac.jp, miyasaka@imr.tohoku.ac.jp*
[b] *Department of Chemistry, Graduate School of Science, Kyushu University, Motooka 744, Nishi-ku, Fukuoka 819-0395, Japan*
[c] *Institute for Chemical Reaction Design and Discovery (WPI-ICReDD), Hokkaido University, Kita 21, Nishi 10, Kita-ku, Sapporo 001-0021, Japan*

† Electronic supplementary information (ESI) available: Experimental, crystallographic data, SEM, PXRD patterns, FT-IR spectra, TGA curve, UV-vis reflectance spectra and computational analysis. CCDC 2235241, 2235242 and 2235244–2235247. For ESI and crystallographic data in CIF or other electronic format see DOI: https://doi.org/10.1039/d3cc00179b

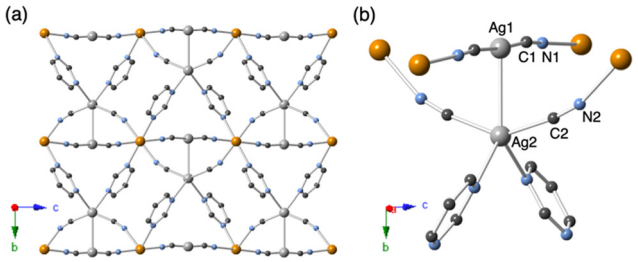

Fig. 1 Crystal structure of **1** at 300 K. (a) The view is along the *a*-axis. (b) Coordination environment of Ag sites in **1**. Atomic code: Cd, orange; Ag, light grey; C, grey; N, blue. H atoms are omitted for clarity.

Fig. S1, ESI†). The Cd^{2+} ions in **1** are hexa-coordinated with octahedral geometry, where two pmd ligands coordinated to the axial sites of Cd^{2+}, and the other four were bridged by the cyanides of the $[Ag(CN)_2]^-$ species (Fig. S1(a), ESI†). More specifically, half of the Ag^+ ions in **1** adopt a linear geometry (labelled as Ag1 in Fig. 1(b)), whereas the others have tetrahedral structures (labelled as Ag2). Furthermore, the distance between the Ag1···Ag2 atoms ($d_{Ag1\cdots Ag2}$) at 300 K is 3.0033(5) Å, which is shorter than twice the van der Waals radius of the Ag^+ ion (3.44 Å), indicating the presence of argentophilic interactions in the framework.[24,25] The chemical formula and phase purity of **1** were confirmed by elemental analysis, powder X-ray diffraction (PXRD) patterns (Fig. S2(a), ESI†), and thermogravimetric analysis (TGA) (Fig. S2(c), ESI†). Infrared (IR) spectra showed the two stretching modes of bridging CN^- ligands at 2126 cm^{-1} and 2160 cm^{-1} (Fig. S2(b), ESI†), corresponding to the two different cyanide coordination modes in **1** (Fig. 1(b)).

The thermal expansion (TE) of **1** was investigated using VT-SCXRD (Fig. 2 and Table S1, ESI†) and VT-synchrotron PXRD measurements (Fig. S3, ESI†) because the luminescent properties of the d^{10} and d^8 systems (Au^I, Ag^I, Cu^I, and Pt^{II}) tend to be closely related to changes in the metallophilicity of their emission centres with temperature variation.[26–32] The obtained TE coefficients with standard deviation (SD) for the respective axes and volumes are summarised in Fig. 2. **1** displays anisotropic TE behaviour, which comprises positive TE and negative TE with coefficients of α_a = +12.5(2.4) MK^{-1} (MK^{-1} = 10^{-6} K^{-1}), α_b = +53.5(3.6) MK^{-1}, α_c = −23.1(7.6) MK^{-1}, and α_{volume} = +44.9(8.2) MK^{-1}, where the coefficient of thermal expansion $\alpha = dl/ldT$ (l = lattice parameter). Such an anisotropic TE behaviour is often observed in cyanide-bridged CPs/MOFs due to relatively weak interactions, framework topologies, and various external stimuli.[33–40] It is noted that the TE coefficient in the *b* axis related to $d_{Ag1\cdots Ag2}$ is the largest of the values in these three axes. Additionally, the $d_{Ag1\cdots Ag2}$ value systematically decreased from 3.0033(5) Å at 300 K to 2.9877(4) Å at 100 K during cooling (Fig. S4, ESI†).

Photophysical measurements of **1** were conducted to explore the relationship between its structure and luminescence characteristics. Fig. 3(a) shows the VT-emission spectra. At 300 K, **1** exhibited a broad emission with a maximum of λ_{em} = 481 nm upon excitation at λ_{ex} = 330 nm. In addition, the VT-emission spectra gradually red-shifted from 481 to 501 nm, accompanied by the enhancement of the luminescence intensity with cooling. As shown in Fig. 3(b), the VT-excitation spectra measured at λ_{em} = 481–501 nm were similar in shape and rapidly fell around 340 nm, indicating the same luminescence origin in all temperature ranges. The VT-emission decay curves display exponential behaviour with lifetimes in the order of microseconds of 14.1 μs (300 K), 22.1 μs (250 K), 26.5 μs (200 K), 28.7 μs (150 K), 29.6 μs (100 K) and 30.1 μs (77 K) (Fig. 3(c)). These results imply that the resultant emission profiles have a spin-forbidden triplet origin, in which the nonradiative decay process was diminished with cooling.[41,42] Moreover, the emission maximum energy of **1** exhibited a good relationship with $d_{Ag1\cdots Ag2}$

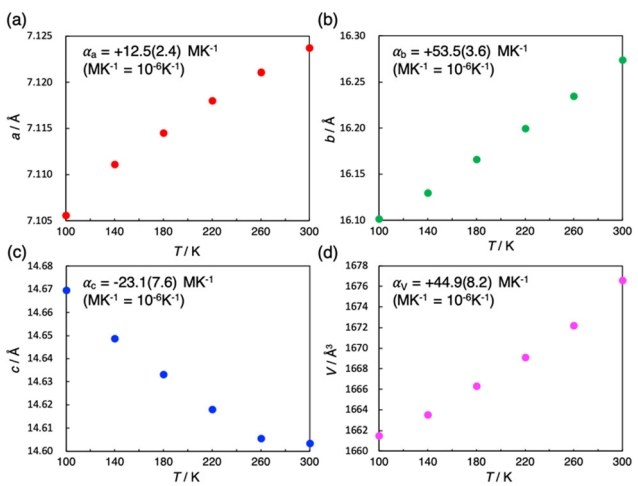

Fig. 2 Thermal variation of cell parameters and thermal expansion constants (MK^{-1} = 10^{-6} K^{-1}) with standard deviation (SD): (a) *a*-, (b) *b*-, and (c) *c*-axis and (d) volume calculated using VT-SCXRD results (100–300 K).

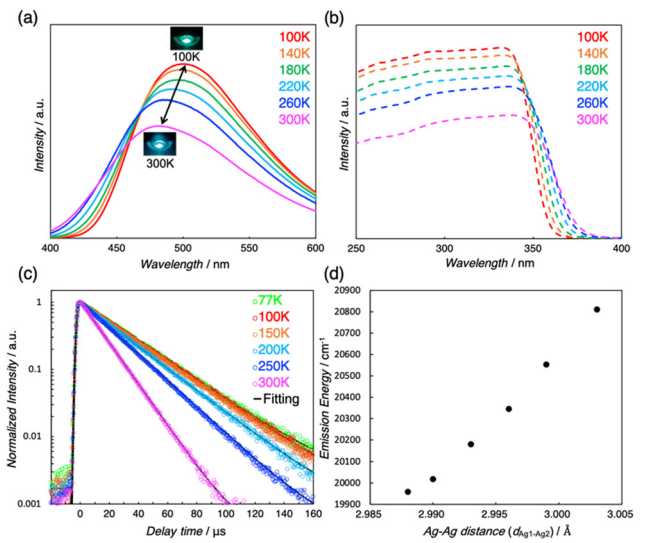

Fig. 3 (a) VT-emission spectra (λ_{ex} = 330 nm). Photographs of **1** at 100 K and 300 K are shown in the inset. (b) VT-excitation spectra (λ_{em} = 481–501 nm) of **1**. (c) VT-emission decay curves (λ_{ex} = 350 nm) of **1**. (d) Plot of emission maximum energy (cm^{-1}) *vs.* $d_{Ag1\cdots Ag2}$ (Å).

(Fig. 3(d)), indicating the contribution of Ag–Ag sites to the luminescence properties.

Surprisingly, the emission intensity of **1** was quite strong even at RT, and the photoluminescence quantum yield (Φ_{em}) was approximately 60%. To the best of our knowledge, the resultant Φ_{em} of **1** is the highest value at RT for phosphorescent Ag-based CPs or MOFs. To further investigate the deeper insights into the emission properties of **1**, we carried out DFT calculations using the SCXRD data at 300 K as a structural model (details of the DFT calculations are summarized in the ESI†). The optimised infinite structure of **1** at the ground state (S_0) provided reasonable cell parameters compared to the SCXRD data of **1** at 300 K (Fig. 4(a)); a discrete model structure cut from the optimised infinite form, where the pmd ligands were terminated by hydrogen atoms, was used for the S_0 calculation (Fig. 4(b) and Table S2, ESI†). The calculated molecular orbitals (MOs) related to the electronic transitions suggest that the luminescent feature of **1** is derived from both the Ag···Ag units and pmd ligands, where, for the S_0 state, the highest occupied MO (HOMO) possesses a clear σ^*_{Ag-Ag} character formed by Ag d orbitals, and the lowest unoccupied MO (LUMO) is the π^* orbital of the pmd ligands (Fig. 4(b)). Moreover, a roughly calculated T_1 state also agreed with this orbital configuration along with a contraction of the M···M distance at the excited state (Fig. S5 and Table S2, ESI†), although the incorporation of the effects from surrounding charges and the resulting electric field through the charge embedding method should be required to discuss properly the relaxation of the T_1 states.[43] Thus, the luminescence origin of **1** can be ascribed to metal–metal-to-ligand charge transfer (MMLCT) transitions, which are sometimes observed in d^{10} or d^8 multinuclear luminescence compounds.[44–46] Generally, MMLCT-based emissions are driven by the collaboration of close metallophilic interactions and ligands with appropriate π^* orbitals.[47–50] Hence, the resultant computational analysis indicated that **1** also exhibited a similar trend to the previously reported MMLCT character.

Finally, we studied the effect of MMLCT on the luminescence efficiency of **1**. Compound **1** shows a significantly high Φ_{em} value of approximately 60% at RT compared with the previous highest Φ_{em} of 22% for the recently reported phosphorescent Ag-MOF of type $\{[Ag_2L_2(CH_3CN)_2](BF_4)_2\}_n$ (**2**; L = diphenyl(2-pyrazyl)phosphine) with the previous highest Φ_{em} of 22% at RT.[51] Compound **2** is a 3D framework involving

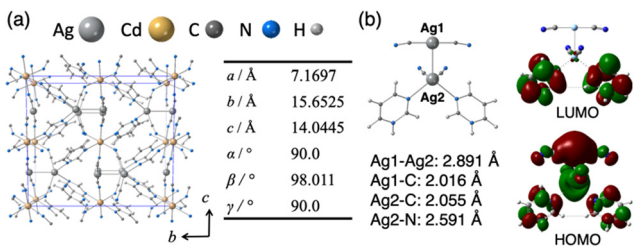

Fig. 4 (a) Infinite optimised structure and cell parameters of **1** at the ground S_0 state by DFT calculations. (b) Calculated MOs of the model for **1** at the S_0 state.

Table 1 Comparison of photophysical properties for **1** and $\{[Ag_2L_2(CH_3CN)_2](BF_4)_2\}_n$ (**2**)[51] in the solid state at 300 K

	1 (300 K)	**2** (300 K)[51]
$\lambda_{em}{}^a$/nm	487	545
$\Phi_{em}{}^b$	0.596	0.22
$\tau_{em}{}^c$/μs	14.1	139
$k_r{}^d$/s^{-1}	4.23×10^4	1.58×10^3
$k_{nr}{}^e$/s^{-1}	2.87×10^4	5.61×10^3
k_r/k_{nr}	1.48	0.282

[a] Emission maximum. [b] Photoluminescence quantum yields. [c] Emission lifetime. [d] Radiative decay rate constants (k_r) were estimated using the equation: Φ_{em}/τ_{em}. [e] Nonradiative decay rate constants (k_{nr}) were estimated using the equation: $k_r(1 - \Phi_{em})/\Phi_{em}$.

$[Ag_2L_2(MeCN)_2]$ building units (Fig. S6, ESI†), in which the emission mechanism of **2** was assigned to intraligand phosphorescence (^{3}IL). By employing **2**, we discuss the effects of different emission mechanisms on the photoluminescence quantum yield. Photophysical parameters such as Φ_{em}, emission lifetimes (τ_{em}), radiative decay rate constants (k_r), and nonradiative decay rate constants (k_{nr}) of **1** and **2** at 300 K are summarised in Table 1.

Notably, the τ_{em} value of **1** was significantly smaller than that of **2**, indicating that, due to heavy-atom effects, the radiative deactivation of **1**, including intersystem crossing, is more efficient (Table 1). Moreover, the k_r and k_{nr} values of **1** were approximately 26 and 5 times larger than those of **2**, respectively. The relatively small k_{nr} of **1** might be attributed to the coordination environment of the Ag ions, as well as the kind of Ag-surrounding ligands and the rigidity of the framework. Importantly, d^{10} metal ions with a closed-shell electronic configuration can form a variety of coordination geometries,[10,52] which significantly influences the emission properties as demonstrated in an Au^I-based complex.[53] Thus, the Ag···Ag-related emission path and structural rigidity of the tetrahedral Ag2 ions in **1** would be key factors for the highest Φ_{em} value.

In summary, we have reported a new phosphorescent Ag-CP of type $[Cd^{II}(pmd)\{Ag^I(CN)_2\}_2]$ (**1**; pmd = pyrimidine) with an intensive phosphorescence originating from MMLCT transitions. The high luminescence quantum efficiency (Φ_{em} = 59.6%) of Ag-based CPs at RT might be due to the effective luminescent path involving Ag–Ag contacts and the structural rigidity of the framework, including the coordination mode of Ag^+ ions. We highlight that luminescent CPs with the ^{3}MMLCT character can be promising for novel photofunctional materials because of their attractive possibilities such as highly efficient luminescence and favourable emission lifetimes.

H. Y. designed the project and performed all lab experiments and VT-synchrotron PXRD at SAGA-LS. M. S., K. M., and K. O. carried out photoluminescence lifetime measurements. J.P. and Y. H. performed the computational analysis. W. K. assisted in VT-emission and excitation spectroscopy measurements. H. Y. and H. M. edited the manuscript.

This work was supported by a Grant-in-Aid for Scientific Research (No. 18H05208, 20H00381, 20H05676, 20J21226, 21K18925, 21K14590, and 21K18970) from MEXT, Japan; the

GIMRT program; the E-IMR project at IMR, Tohoku University, the Noguchi Institute; and the R4 Young Researchers Support Project, Faculty of Science, KYUSHU UNIVERSITY (Grant number 22-A5). H. Y. is thankful to the Iketani Science and Technology Foundation (No. 0341161-A) and Izumi Science and Technology Foundation (No. 2022-J-076). The VT-synchrotron PXRD measurements were performed at BL-15 of the SAGA Light Source (proposal no. 2205035F). The authors thank Prof. Dr Tetsu Ichitsubo and Dr Hongyi Li for their kind support with scanning electron microscopy (SEM) measurements. The authors also thank Dr Masaki Yoshida for useful discussions regarding the interpretation of luminescent properties.

Conflicts of interest

There are no conflicts to declare.

References

1 M. Irie, T. Fukaminato, T. Sasaki, N. Tamai and T. Kawai, *Nature*, 2002, **420**, 759.
2 X. Zhang, S. Rehm, M. M. Safont-Sempere and F. Würthner, *Nat. Chem.*, 2009, **1**, 623.
3 P. Kumar, S. Singh and B. K. Gupta, *Nanoscale*, 2016, **8**, 14297.
4 D. Jariwala, V. K. Sangwan, L. J. Lauhon, T. J. Marks and M. C. Hersam, *Chem. Soc. Rev.*, 2013, **42**, 2824.
5 C. D. S. Brites, S. Balabhadra and L. D. Carlos, *Adv. Opt. Mater.*, 2019, **7**, 1801239.
6 S. Medici, M. Peana, G. Crisponi, V. M. Nurchi, J. I. Lachowicz, M. Remelli and M. A. Zoroddu, *Coord. Chem. Rev.*, 2016, **327**, 349.
7 R. A. D. Arancon, A. M. Balu, A. A. Romero, M. Ojeda, M. Gomez, J. Blanco, J. L. Domingo and R. Luque, *Environ. Res.*, 2017, **154**, 204.
8 K. Kennes, C. Martin, W. Baekelant, E. Coutino-Gonzalez, E. Fron, M. B. J. Roeffaers, J. Hofkens and M. Van der Auweraer, *ACS Appl. Mater. Interfaces*, 2019, **11**, 12179.
9 S. Horiuchi, S. Moon, A. Ito, J. Tessarolo, E. Sakuda, Y. Arikawa, G. H. Clever and K. Umakoshi, *Angew. Chem., Int. Ed.*, 2021, **60**, 10654.
10 V. W. Yam and K. K. Lo, *Chem. Soc. Rev.*, 1999, **28**, 323.
11 Z. Wei, X.-H. Wu, P. Luo, J.-Y. Wang, K. Li and S.-Q. Zang, *Chem. – Eur. J.*, 2019, **25**, 2750.
12 J.-H. Jia, D. Liang, R. Yu, X.-L. Chen, L. Meng, J.-F. Chang, J.-Z. Liao, M. Yang, X.-N. Li and C.-Z. Lu, *Chem. Mater.*, 2020, **32**, 620.
13 M. J. Katz, T. Ramnial, H.-Z. Yu and D. B. Leznoff, *J. Am. Chem. Soc.*, 2008, **130**, 10662.
14 A. Lan, K. Li, H. Wu, D. H. Olson, T. J. Emge, W. Ki, M. Hong and J. Li, *Angew. Chem., Int. Ed.*, 2009, **48**, 2334.
15 N. Yanai, K. Kitayama, Y. Hijikata, H. Sato, R. Matsuda, Y. Kubota, M. Takata, M. Mizuno, T. Uemura and S. Kitagawa, *Nat. Mater.*, 2011, **10**, 787.
16 Y. Takashima, V. M. Martínez, S. Furukawa, M. Kondo, S. Shimomura, H. Uehara, M. Nakahama, K. Sugimoto and S. Kitagawa, *Nat. Commun.*, 2011, **2**, 168.
17 N. B. Shustova, A. F. Cozzolino, S. Reineke, M. Baldo and M. Dincă, *J. Am. Chem. Soc.*, 2013, **135**, 13326.
18 R.-B. Lin, S.-Y. Liu, J.-W. Ye, X.-Y. Li and J.-P. Zhang, *Adv. Sci.*, 2016, **3**, 1500434.
19 W. P. Lustig, S. Mukherjee, N. D. Rudd, A. V. Desai, J. Li and S. K. Ghosh, *Chem. Soc. Rev.*, 2017, **46**, 3242.
20 Y. Zhang, S. Yuan, G. Day, X. Wang, X. Yang and H.-C. Zhou, *Coord. Chem. Rev.*, 2018, **354**, 28.
21 B. R. Varju, S. A. Wollschlaeger and D. B. Leznoff, *Chem. – Eur. J.*, 2019, **25**, 9017.
22 X.-Y. Liu, W. P. Lustig and J. Li, *ACS Energy Lett.*, 2020, **5**, 2671.
23 M. Gutiérrez, C. Martín, B. E. Souza, M. V. Auweraer, J. Hofkens and J.-C. Tan, *Appl. Mater. Today*, 2020, **21**, 100817.
24 P. Pyykkö, *Chem. Rev.*, 1997, **97**, 597.
25 H. Schmidbaur and A. Schier, *Angew. Chem., Int. Ed.*, 2015, **54**, 746.
26 T. H. Kim, Y. W. Shin, J. H. Jung, J. S. Kim and J. Kim, *Angew. Chem., Int. Ed.*, 2008, **47**, 685.
27 S. Perruchas, X. F. Le Goff, S. Maron, I. Maurin, F. Guillen, A. Garcia, T. Gacoin and J.-P. Boilot, *J. Am. Chem. Soc.*, 2010, **132**, 10967.
28 I. O. Koshevoy, C.-L. Lin, A. J. Karttunen, M. Haukka, C.-W. Shih, P.-T. Chou, S. P. Tunik and T. A. Pakkanen, *Chem. Commun.*, 2011, **47**, 5533.
29 B. Li, R.-W. Huang, J.-H. Qin, S.-Q. Zang, G.-G. Gao, H.-W. Hou and T. C. W. Mak, *Chem. – Eur. J.*, 2014, **20**, 12416.
30 M. Jin, T. S. Chung, T. Seki, H. Ito and M. A. Garcia-Garibay, *J. Am. Chem. Soc.*, 2017, **139**, 18115.
31 M. Jin, S. Yamamoto, T. Seki, H. Ito and M. A. Garcia-Garibay, *Angew. Chem.*, 2019, **131**, 18171.
32 D. Saito, T. Ogawa, M. Yoshida, J. Takayama, S. Hiura, A. Murayama, A. Kobayashi and M. Kato, *Angew. Chem., Int. Ed.*, 2020, **59**, 18723.
33 S. Margadonna, K. Prassides and A. N. Fitch, *J. Am. Chem. Soc.*, 2004, **126**, 15390.
34 K. W. Chapman and P. J. Chupas, *J. Am. Chem. Soc.*, 2007, **129**, 10090.
35 A. L. Goodwin, M. Calleja, M. J. Conterio, M. T. Dove, J. S. O. Evans, D. A. Keen, L. Peters and M. G. Tucker, *Science*, 2008, **319**, 794.
36 J. L. Korčok, M. J. Katz and D. B. Leznoff, *J. Am. Chem. Soc.*, 2009, **131**, 4866.
37 J. Chen, L. Hu, J. Deng and X. Xing, *Chem. Soc. Rev.*, 2015, **44**, 3522.
38 J. S. Ovens and D. B. Leznoff, *Inorg. Chem.*, 2017, **56**, 7332–7343.
39 B. R. Mullaney, L. Goux-Capes, D. J. Price, G. Chastanet, J.-F. Létard and C. J. Kepert, *Nat. Commun.*, 2017, **8**, 1053.
40 R. Ohtani, H. Yoshino, J. Yanagisawa, H. Ohtsu, D. Hashizume, Y. Hijikata, J. Pirillo, M. Sadakiyo, K. Kato, Y. Shudo, S. Hayami, B. Le Ouay and M. Ohba, *Chem. – Eur. J.*, 2021, **27**, 18135.
41 M. D. Allendorf, C. A. Bauer, R. K. Bhakta and R. J. T. Houk, *Chem. Soc. Rev.*, 2009, **38**, 1330.
42 Y. Cui, Y. Yue, G. Qian and B. Chen, *Chem. Rev.*, 2012, **112**, 1126.
43 Z. Tu, G. Han, T. Hu, R. Duan and Y. Yi, *Chem. Mater.*, 2019, **31**, 6665.
44 A. Aliprandi, M. Mauro and L. De Cola, *Nat. Chem.*, 2016, **8**, 10.
45 S. Carrara, A. Aliprandi, C. F. Hogan and L. De Cola, *J. Am. Chem. Soc.*, 2017, **139**, 14605.
46 M. Yoshida and M. Kato, *Coord. Chem. Rev.*, 2018, **355**, 101.
47 J. C. Deaton, A. Chakraborty, R. Czerwieniec, H. Yersin and F. N. Castellano, *Phys. Chem. Chem. Phys.*, 2018, **20**, 25096.
48 M. Jin, T. Sumitani, H. Sato, T. Seki and H. Ito, *J. Am. Chem. Soc.*, 2018, **140**, 2875.
49 D. J. Shields, T. Elkoush, E. Miura-Stempel, C. L. Mak, G.-H. Niu, A. D. Gudmundsdottir and M. G. Campbell, *Inorg. Chem.*, 2020, **59**, 18338.
50 T. Seki, K. Ida, H. Sato, S. Aono, S. Sakaki and H. Ito, *Chem. – Eur. J.*, 2020, **26**, 735.
51 M. I. Rogovoy, A. S. Berezin, D. G. Samsonenko and A. V. Artem'ev, *Inorg. Chem.*, 2021, **60**, 6680.
52 C.-M. Che, M.-C. Tse, M. C. W. Chan, K.-K. Cheung, D. L. Phillips and K.-H. Leung, *J. Am. Chem. Soc.*, 2000, **122**, 2464.
53 K. Igawa, N. Yoshinari, M. Okumura, H. Ohtsu, M. Kawano and T. Konno, *Sci. Rep.*, 2016, **6**, 26002.